# DETECTION AND ISOLATION OF A MULTIPLICATIVE FAULT IN A WIRELESS POWER TRANSFER SYSTEM

**Dejan Janjic[1], Sanja Antic[1], Branko Koprivica[1]**

[1] *University of Kragujevac, Faculty of technical sciences Čačak*

**Abstract**

*The experimental procedure presented in the paper focuses on detecting and isolating the multiplicative fault of the compensating capacitor which can occur due to certain application conditions, on a wireless energy transfer system model. The testing was conducted on a laboratory system, which involved measuring changes in voltages and currents based on the change in the compensating capacitor's value (simulating a fault). The results obtained from the efficiency curve at the resonant frequency for different compensating capacitor values were used to detect and isolate the multiplicative fault. Additionally, the same curve was used in the approximate fault identification process, which involved determining the fault's size.*

**Keywords:** wireless energy transfer, detection and isolation of multiplicative fault, efficiency, a resonant circuit with series-parallel compensation.

## INTRODUCTION

With the growing complexity of control systems, the issue of their security and robustness has become more prominent in various processes [1]–[5]. The reliability, robustness, availability, and environmental safety of such systems are mainly expressed through their sensitivity to random faults. As a result, a discipline of fault detection and isolation (FDI) has been developed in engineering theory and practice to address these concerns.

Faults can be broadly defined as deviations from normal system behavior. However, in engineering, two specific types of faults are of interest: additive and multiplicative. Additive faults are unknown, input signals that affect system response and are desirable for detection [6]. Multiplicative faults are changes in process parameters that occur during operation.

Fault detection and isolation involve three primary tasks that must be solved. The first task is to identify the presence of a fault, which is performed by detecting any abnormal operation in the system. The second task is to locate the occurrence of the fault, which is referred to as fault isolation. The third task is fault identification, which involves determining the severity of the fault. Fault isolation and identification are collectively referred to as fault diagnosis. While fault detection is necessary for all practical processes, and fault isolation is almost as important, fault identification is often difficult to implement. Due to this, many practical systems only include fault detection and isolation (FDI), and the term "diagnosis" is often used synonymously with "isolation".

The foundations for the implementation of the system for wireless energy transmission using the resonance method are analyzed in detail in the literature [7]. Investigation of the coil parameter, on the wireless power transfer efficiency at greater air gaps and different receiver capacitance for electric vehicle applications is discussed in [5]. A study on transmission coil parameters for wireless power transfer in electric vehicles is given in [8].

A design of method proposed to determine the operating modes of a high-efficiency inductive wireless power transfer

system that can support multiple receivers is presented in [9]. The operating modes are no-load, safe, and fault modes. The paper [10] presents a wireless power transfer (WPT) system that uses a dual-coupled inductor-capacitor-capacitor and series (LCC-S) compensation method to improve the misalignment performance and achieve fault tolerant operation. The proposed system also features a compact receiver size and ensures stable output power.

In the paper, a system for wireless energy transmission based on the application of the resonance method is implemented. The results of experimental testing of the laboratory system for wireless power transfer, as well as the procedure of experimental detection and isolation of a multiplicative fault due to compensating capacitor change, which can occur during certain operating conditions, are given.

The paper is organized as follows: after the description of the laboratory system, its mathematical model is given, followed by a presentation of the experimental results and a conclusion.

## THE LABORATORY SYSTEM SETUP

The block diagram of the laboratory system for wireless power transfer is shown in Fig.1.

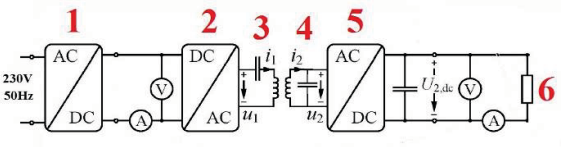


***Fig. 1.*** *The block diagram of the laboratory system for wireless power transfer*

The system consists of the following components: 1) DC voltage source of 0-30 V, 5 A, 2) DC/AC voltage converter, 3) series connections of the transmitting coil and compensating capacitor, 4) parallel connections of the receiving coil and compensating capacitor, 5) AC voltage rectifier and 6) receiver in the form of ohmic resistance.

A DC voltage of 12 V from DC voltage source 1 is supplied to the input of DC/AC converter 2 which generates a rectangular AC voltage of amplitude 0-30 V at frequencies from 15 kHz to 120 kHz. This AC voltage is supplied the transmitting coil 3, which is coupled to the receiving coil 4. At the output of the receiving coil 4, an AC voltage of a frequency equal to the frequency of the voltage connected to the transmitting coil 3 appears. The AC voltage from the coil 4 is rectified in the rectifier 5 and supplied to receiver 6.

The described system is shown in Fig. 2. The dimensions and electrical parameters data of the coil system, are given in Table 1. The coils have the same dimensions and inductance, and the compensating capacitors have the same capacitance. Their inductances and capacitances were measured with a PeakTech 2170 universal RLC bridge. The mutual inductance of the coils was not determined.

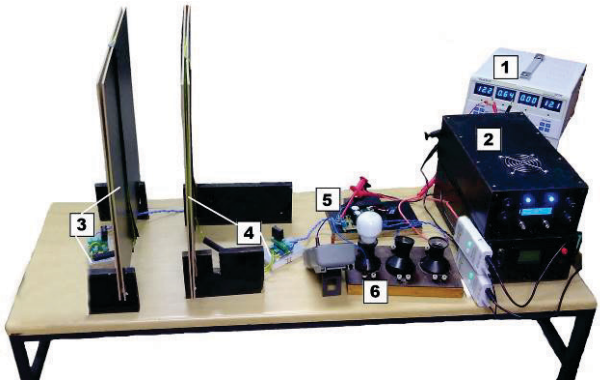


***Fig. 2.*** *The laboratory system setup for wireless power transfer*

***Table 1****. System parameters*

| | |
|---|---|
| The inner diameter of the coils [mm] | 375 |
| The outer diameter of the coils [mm] | 440 |
| $L_1$, $L_2$ [μH] | 100 |
| $C_1$, $C_2$ [nF] | 300 |

Only one capacitor, $C_1$, had its compensating capacitor value changed.

## MATHEMATICAL MODEL OF THE SYSTEM

The realization of the system for wireless power transfer is based on the application of the resonance method. This

method implies the existence of reactive (inductive and capacitive) parts in the transmitting and receiving circuit, for the system to work in resonant conditions. Due to the dimensions of the coils, the parasitic capacitance is not sufficient to ensure resonance in the operating frequency range, determined by the application of the wireless transfer system. Accordingly, to achieve resonance in the desired frequency range, it is necessary to add reactive elements (most often capacitors) on the transmitting and receiving side, which is characterized as an additional compensation network. Thus, series-series, series-parallel, parallel-series, and parallel-parallel compensation methods can be realized.

In the observed system, a resonant circuit with series-parallel compensation was applied, the connection diagram of which is shown in Fig. 3.

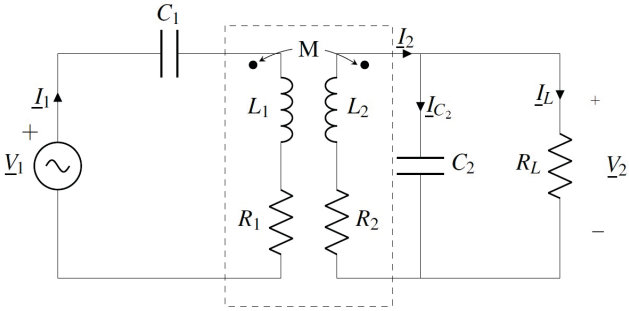


***Fig. 3.*** *Connection diagram of a resonant circuit with series-parallel compensation*

For the coupled circuit from Fig.3, the following equations can be written according to Kirchhoff's I and II laws:

$$\underline{I}_2 = \underline{I}_{C2} + \underline{I}_L,$$

$$\underline{V}_1 = \left( R_1 + j\omega L_1 + \frac{1}{j\omega C_1} \right) \underline{I}_1 - j\omega M \underline{I}_2, \quad (1)$$

$$\underline{V}_2 = -\left( R_2 + j\omega L_2 \right) \underline{I}_2 + j\omega M \underline{I}_1 = R_L \underline{I}_L = \frac{\underline{I}_{C_2}}{j\omega C_2}.$$

where: ω is angular frequency, $\underline{V}_1$, $\underline{V}_2$, $\underline{I}_1$, $\underline{I}_2$, are voltages and currents of the primary and secondary circuits respectively, $\underline{I}_{C2}$, $\underline{I}_L$ are condenser and resistance currents at the output of the secondary circuit, $L_1$, $L_2$, are inductances of the transmitting and receiving coils, $R_1$, $R_2$ are parasite resistances of the coils, $R_L$ is receiver resistance, $M$ is mutual inductance, $C_1$, $C_2$ are compensating capacitances of the primary and secondary circuits.

Based on (1), the input impedance of the system is obtained in the form:

$$\underline{Z}_{ul} = \frac{\underline{V}_1}{\underline{I}_1} = \left( R_1 + j\omega L_1 + \frac{1}{j\omega C_1} \right) + \frac{\omega^2 M^2 \left( j\omega C_2 R_L + 1 \right)}{R_L + \left( R_2 + j\omega L_2 \right)\left( j\omega C_2 R_L + 1 \right)}. \quad (2)$$

The imaginary part of the input impedance is:

$$\mathrm{Im}\left( \underline{Z}_{ul} \right) = \omega L_1 - \frac{1}{\omega C_1} + \frac{\omega^3 M^2 L_2 \left( C_2 R_2 - 1 - \omega^2 L_2 C_2 R_2 \right)}{\left( R_L + R_2 - \omega^2 L_2 C_2 R_L \right)^2 + \omega^2 \left( L_2 + C_2 R_2 R_L \right)^2}. \quad (3)$$

Relation (3) can be simplified by neglecting the parasite resistance of the secondary coil $R_2$, as its numerical value is much smaller than the resistance of the receiver $R_L$:

$$\mathrm{Im}\left( \underline{Z}_{ul} \right) = \omega L_1 - \frac{1}{\omega C_1} - \frac{\omega^3 M^2 L_2}{\left( R_L - \omega^2 L_2 C_2 R_L \right)^2 + \omega^2 L_2^2}. \quad (4)$$

The circuit's resonant frequencies can be now found by setting the imaginary part of the input impedance (4), to zero.

When the primary and secondary coils are at a sufficient distance, the mutual inductance can be neglected, $M \approx 0$, so based on relations (3), i.e. (4), the resonant frequency depends only on the parameter of the primary circuit (inductance $L_1$ of the receiving coil and compensation capacitance $C_1$),

$$\omega_r = \frac{1}{\sqrt{L_1 C_1}}. \quad (5)$$

Based on the values given in Table 1, it follows:

$$\omega_r = 29\,\text{kHz}\,. \qquad (6)$$

At smaller distances between the coils, when the mutual inductance $M$, defined with:

$$M = k\sqrt{L_1 L_2}, k \le 1, \qquad (7)$$

cannot be neglected, taking into account $C_1$=$C_2$, $L_1$=$L_2$ (Table 1), and numerous parameters values, at $\omega$=$\omega_r$, (4) becomes:

$$\text{Im}\left(\underline{Z}_{ul}\right) = -\frac{\omega_r M^2}{L_2} \approx 0. \qquad (8)$$

So the resonant frequency can still be considered unchanged, given by (5).

## EXPERIMENTAL RESULTS

Through experimental testing, it is determined that the output voltage changes according to a complex law with the change of the distance between the coils and the frequency. To examine in more detail the detection and isolation of the multiplicative fault, it is determined that the examination is performed at only one distance of the wireless transmitter and receiver coil $d$=15cm. At the same time, the frequency is changed with a step of 1 kHz (starting from 20 kHz to 40 kHz), and the simulation of multiplicative fault on the compensation capacitor $C_1$ is realized by changing its value with a step of 50nF (starting from 100nF to 700nF).

The performance test of the implemented system for wireless power transfer was performed with a passive load (6), a resistor of 100 Ω, and a power of 100 W.

DC voltage measurements were made with a digital voltmeter at the output of the rectifier 5, which is also the voltage of the receiver 6, and the system frequency was measured using a Hantek 6074 DB four-channel USB oscilloscope.

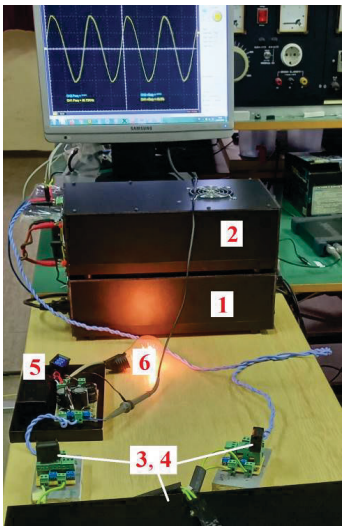


***Fig. 4**. The system frequency measurement*

Fig.4 shows the realized laboratory setup and the system frequency measurement. It can been see that the signal on the receiving coil 4 before the AC/DC rectifier 5, is sinusoidal.

The simulation of multiplicative fault on capacitor $C_1$ was performed by forming different groups of capacitors, the combination of which obtained the desired value of $C_1$. Groups of capacitors were placed on the circuit board, with connectors connected in parallel, and after obtaining the required values, measurements were made with a range of frequencies.

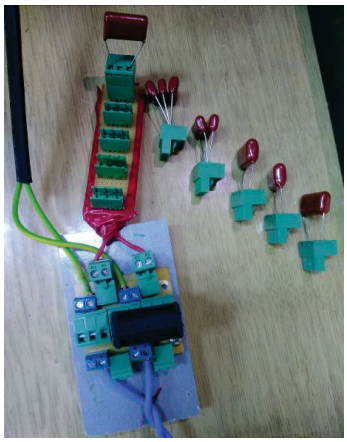

***Fig.5**. Plates with connectors for compensating capacitors and formed groups of capacitors*

Table 2 shows the results of one set of measurements for the value of the nominal compensation capacitor $C_1$=300nF. The values of measured frequency $f$, DC current

$I_1$, DC voltage $U_2$, and DC current $I_2$ are shown.

***Table 2.*** *The measurement results for* $U_1$=12 V, $C_1$=300nF, $d$=15 cm

| $f$ (Khz) | $I_1$ (A) | $U_2$ (V) | $I_2$ (A) |
|---|---|---|---|
| 40 | 0.12 | 3.70 | 0.035 |
| 39 | 0.14 | 4.00 | 0.043 |
| 38 | 0.16 | 5.30 | 0.053 |
| 37 | 0.23 | 6.70 | 0.067 |
| 36 | 0.33 | 8.80 | 0.084 |
| 35 | 0.50 | 11.40 | 0.113 |
| 34 | 0.73 | 14.80 | 0.144 |
| 33 | 1.12 | 21.00 | 0.202 |
| 32 | 1.53 | 27.70 | 0.266 |
| 31 | 1.83 | 32.30 | 0.311 |
| 30 | 1.94 | 34.70 | 0.335 |
| 29 | 1.89 | 35.80 | 0.341 |
| 28 | 1.62 | 33.60 | 0.326 |
| 27 | 1.36 | 30.10 | 0.292 |
| 26 | 1.08 | 25.70 | 0.248 |
| 25 | 0.80 | 21.00 | 0.202 |
| 24 | 0.43 | 13.60 | 0.131 |
| 23 | 0.26 | 8.80 | 0.086 |
| 22 | 0.17 | 6.40 | 0.058 |
| 21 | 0.12 | 4.00 | 0.038 |
| 20 | 0.11 | 2.70 | 0.024 |

From the results given in Table 2, the input and output active power of the system, as well as the system efficiency η, were calculated. These results are shown in Table 3.

One measurement set had 21 individual measurements of the system input and output parameters. For this study, 13 measurement sets were performed, which gives a total of 273 individual measurements.

Based on these measurements, a 3D diagram of the efficiency of the system as a function of the compensation capacitor $C_1$ and the frequency was created and is shown in Fig.6.

Analyzing the 3D efficiency diagram, it can be seen that the maximum efficiency of the system is for the nominal value of the compensation capacitor $C_1$=300nF and the frequency near the resonant, $f$=28kHz (which is the influence of the mutal inductance). It is also observed that when the capacitance $C_1$ changes (simulated fault), there is a sudden drop in the efficiency of the system.

***Table 3.*** *Calculated power and efficiency of the system*

| $f$ (Khz) | $P_{in}$ (W) | $P_{out}$ (W) | η (%) |
|---|---|---|---|
| 40 | 1.440 | 0.130 | 8.99 |
| 39 | 1.680 | 0.172 | 10.24 |
| 38 | 1.920 | 0.281 | 14.63 |
| 37 | 2.760 | 0.449 | 16.26 |
| 36 | 3.960 | 0.739 | 18.67 |
| 35 | 6.000 | 1.288 | 21.47 |
| 34 | 8.760 | 2.131 | 24.33 |
| 33 | 13.440 | 4.242 | 31.56 |
| 32 | 18.360 | 7.368 | 40.13 |
| 31 | 21.960 | 10.045 | 45.74 |
| 30 | 23.280 | 11.625 | 49.93 |
| 29 | 22.680 | 12.208 | 53.83 |
| 28 | 19.440 | 10.954 | 56.35 |
| 27 | 16.320 | 8.789 | 53.86 |
| 26 | 12.960 | 6.374 | 49.18 |
| 25 | 9.600 | 4.242 | 44.19 |
| 24 | 5.160 | 1.782 | 34.53 |
| 23 | 3.120 | 0.757 | 24.26 |
| 22 | 2.040 | 0.371 | 18.20 |
| 21 | 1.440 | 0.152 | 10.56 |
| 20 | 1.320 | 0.065 | 4.91 |

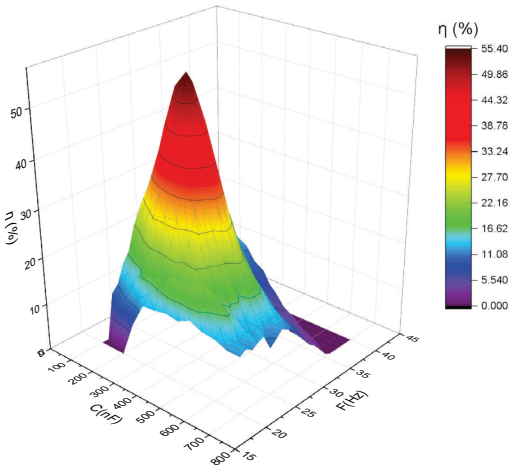


***Fig. 6****. 3D diagram of the system efficiency as a function of the compensation capacitor and the frequency*

Fig. 7 shows the diagram of the system efficiency as a function of the compensation capacitor $C_1$, at the resonant frequency. In this diagram, it can be seen that the maximum efficiency is at the nominal value of $C_1$=300nF and that there are large changes in the efficiency of the system when the capacitance changes.

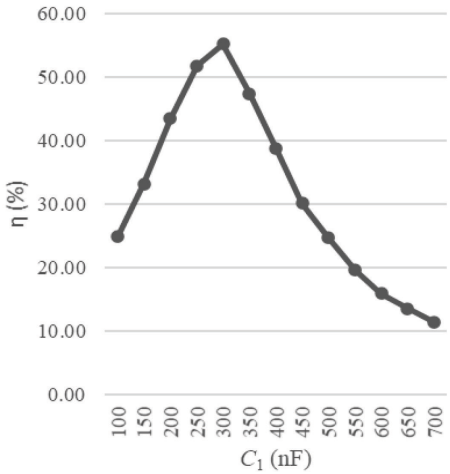


***Fig. 7.*** *Diagram of the system efficiency as a function of the compensation capacitor, at the resonant frequency $f_r$=29kHz*

A change in the capacitance $C_1$ during operation can be considered a multiplicative fault. It can be detected and isolated precisely from the curve of the calculated efficiency of the system at the resonant frequency from Fig.7. Based on the obtained curve, it is also possible to approximately identify the fault by observing the relationship between the drop in efficiency and the size of the change in the capacitance of the capacitor.

Thus, a drop in efficiency of up to 15% is an indication of a capacitance change of approximately ±50nF, and 30% is an indication of a capacitance change of approximately ±100nF. A drop in efficiency of up to 45% is indicative of a capacitance change of approximately ±150nF.

One of the causes of the possible change in the value of the capacitor $C_1$ can be the high temperature the component reached during the opertion. Fig.8 a) shows the compensation capacitor immediately before the system starts, and Fig.8 b) shows it, during system running. The temperature before the system starts was close to the ambient temperature in which the test was performed 22.5ºC, and after some time of operation, the temperature was reached 48.8ºC.

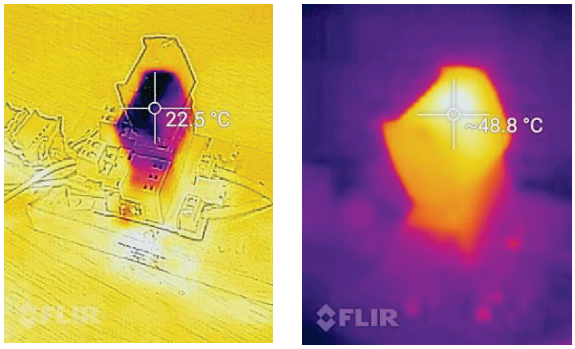


*a)* *b)*

***Fig. 8.*** *Thermal photo of the compensating condenser a) before b)after the system starting*

In real conditions, the cause of the capacitor capacitance change can be the influence of some external or internal factors. Any prolonged operation outside the conditions prescribed by the manufacturer (temperature limit, operating voltage, or life span) can lead to a change in the capacitance of the capacitor, which results in the appearance of a multiplicative fault.

## CONCLUSION

The paper presents the procedure of experimental detection and isolation of a multiplicative fault, caused by the change in capacitance of the compensating capacitor of the primary circuit of the wireless power transfer system. The main parameter in that process represents the efficiency of the system, which was the highest at the nominal capacitance value of $C_1$=300nF and the frequency near the resonant $f$=28kHz and was η=56.35%. The experimental results show that the efficiency drops significantly when changing the capacitance and oscillation frequency. The recorded efficiency curve at resonant frequency and capacitance changes in the range of 100–700nF can be used in the process of approximate

identification of the size of the multiplicative fault.

In real conditions, changes in capacitor capacitance can result from some external or internal factors. This paper presents an effective procedure for detecting and diagnosing this kind of fault.

## REFERENCES


[1] S. A. Mortazavizadeh, M. Ebrahimi, A. Ghaderi, and M. Hajian, "Fault-tolerant control of steer-by-wire systems under voltage and current sensors faults," *Electr. Eng.*, vol. 103, no. 1, pp. 407–415, 2021, doi: 10.1007/s00202-020-01087-3.

[2] S. Antic, V. Luković, and Ž. Đurović, "Expert System for FDI of DC Motor Faults Using Structured Residuals Design Technique," *SJEE*, vol. 20, no. 1, pp. 93–105, Feb. 2023, doi: 10.2298/SJEE2301093A.

[3] C. Urrea and F. Páez, "Design and Comparison of Strategies for Level Control in a Nonlinear Tank," *Process. 2021, Vol. 9, Page 735*, vol. 9, no. 5, p. 735, Apr. 2021, doi: 10.3390/PR9050735.

[4] X. Su and B. Xiao, "Actuator-Integrated Fault Estimation and Fault Tolerant Control for Electric Power Steering System of Forklift," *Appl. Sci. 2021, Vol. 11, Page 7236*, vol. 11, no. 16, p. 7236, Aug. 2021, doi: 10.3390/APP11167236.

[5] Q. He, W. Zhang, P. Lu, and J. Liu, "Performance comparison of representative model-based fault reconstruction algorithms for aircraft sensor fault detection and diagnosis," *Aerosp. Sci. Technol.*, vol. 98, p. 105649, Mar. 2020, doi: 10.1016/J.AST.2019.105649.

[6] S. Antic, M. Rosic, Z. Djurovic, and M. Bozic, "Comparison of structured residuals design techniques for actuator and sensor fault detection and isolation in a permanent magnet DC motor," *Electr. Eng.*, pp. 1–19, Oct. 2023, doi:10.1007/S00202-023-02021-Z/TABLES/12.

[7] A. Triviño-Cabrera, J. M. González-González, and J. A. Aguado, "Wireless Power Transfer for Electric Vehicles: Foundations and Design Approach," 2020, doi: 10.1007/978-3-030-26706-3.

[8] D. K. W. Lo, F. Juwono, W. K. Wong, and I. M. Chew, "A Study on Transmission Coil Parameters for Wireless Power Transfer in Electric Vehicles," *SJEE*, vol. 19, no. 2, pp. 129–145, Jul. 2022, doi: 10.2298/SJEE2202129L.

[9] Z. N. Low, J. J. Casanova, P. H. Maier, J. A. Taylor, R. A. Chinga, and J. Lin, "Method of load/fault detection for loosely coupled planar wireless power transfer system with power delivery tracking," *IEEE Trans. Ind. Electron.*, vol. 57, no. 4, pp. 1478–1486, Apr. 2010, doi: 10.1109/TIE.2009.2030821.

[10] Z. Yan *et al.*, "Fault-Tolerant Wireless Power Transfer System with a Dual-Coupled LCC-S Topology," *IEEE Trans. Veh. Technol.*, vol. 68, no. 12, pp. 11838–11846, Dec. 2019, doi: 10.1109/TVT.2019.2944841.